Advances in Science and Technology Research Journal

Advances in Science and Technology Research Journal, 2025, 19(8), 434–448
https://doi.org/10.12913/22998624/205855
ISSN 2299-8624, License CC-BY 4.0

Received: 2025.04.06
Accepted: 2025.06.15
Published: 2025.07.01

Evaluation of the possibility of obtaining spherical powders of titanium alloy Ti-6Al-4V by supersonic reverse polarity plasma torch for use in additive manufacturing

Shiyi Gao[1*], Volodymyr Korzhyk[1,2], Dmytro Strohonov[2], Oleksii Tereshchenko[2], Oleksii Demianov[2], Oleg Ganushchak[2]

[1] China-Ukraine Institute of Welding, Guangdong Academy of Sciences, Guangdong Provincial Key Laboratory of Material Joining and Advanced Manufacturing: 363, Changxing Road, Tianhe, Guangzhou, 510650, China
[2] E.O. Paton Electric Welding Institute (PEWI), National Academy of Sciences of Ukraine, 11 Kazymyr Malevych St., 03150 Kyiv, Ukraine
* Corresponding author's e-mail: meshiyigao@163.com

ABSTRACT

This work demonstrates the possibility of producing spherical Ti-6Al-4V Grade 5 alloy powders with superior technological properties compared to those obtained through conventional industrial gas atomization methods for additive manufacturing, by utilizing plasma atomization of a 1.0 mm diameter solid wire. The process employs supersonic plasma jets generated by a DC reverse polarity plasma torch with vortex arc stabilization. The plasma torch has a copper hollow electrode-anode and a special diffusive nozzle-cathode. Analysis of the particle size distribution of the powder showed the main fraction of -140 μm 96 wt%, and the amount of the finely-divided fraction of -63 μm is up to 55–60 wt%. Also, using subsonic jet had been give fraction -250 μm, which is 97 wt%, and the amount of the finely-divided fraction -63 μm does not exceed 30 wt%. The study of the shape and structure properties of Ti-6Al-4V Grade 5 powder showed that the sphericity coefficient reaches up to 0.9, the number of defects in the form of satellites and irregular particles does not exceed 1 wt%. In terms of technological characteristics, Ti-6Al-4V Grade 5 powder obtained by the adopted technique is on par with the industrial method of producing spherical powders for additive manufactuing by the direct polarity plasma torches.

Keywords: plasma atomization, reverse polarity, solid wire, Ti alloy, powders, particle size distribution, morphology, technological properties.

INTRODUCTION

The rapid growth of aviation, aerospace, energy, and chemical industries has created a significant demand for manufacturing and repairing of Ti alloy parts, mainly through powder-based additive manufacturing (AM) methods, including selective laser melting (SLM), electron beam melting (EBM), laser direct energy deposition (LDED) and cold spraying (CS) techniques [1–12]. In this case, the properties of the powder feedstock play a primary role in powder-based AM technology, on the process window setup and on the properties of AMed products [13]. All these techniques require spherical metal powders with controlled particle size, high sphericity, low porosity, and good flowability to ensure uniform layer deposition and high-quality final parts [1–4].

The most common method for producing Ti alloy powders is gas atomization (GA) [14], including techniques such as vacuum induction melting inert gas atomization (VIGA) and electrode induction melting inert gas atomization (EIGA). While GA enables relatively high productivity (up to 80 kg/h for VIGA and 20 kg/h for EIGA), it has significant drawbacks: formation of pores due to gas entrapment [15, 16], presence of satellites and irregular particles [17–19], reduced

flowability and packing density [20, 21]. These drawbacks ultimately degraded mechanical properties in AMed parts [23, 24]. An alternative is the plasma rotating electrode process (PREP), which produces powders of excellent sphericity and minimal defects [13, 25, 26]. However, PREP has limitations in scaling and producing fine particles (<106 μm), and it requires precision-machined billets and complex high-speed rotating systems [27–29]. A more promising technique is plasma wire atomization (PA) using three direct polarity plasma torches (3DPT) [30]. This method melts and disperses wire feedstock with converging plasma jets, offering: high control over particle size distribution [31], high finely-divided fraction yield (< 63 μm up to 60 wt%) [32], and flexibility in feedstock materials. Despite these advantages, current PA-3DPT systems are limited by: low productivity (~1.0 kg/h for Ti-6Al-4V alloy) [33], high equipment cost due to multi-arc configuration, and restricted power of existing plasma torches, limiting plasma velocity and melt dispersion [34].

This necessitates the overcoming these limitations by developing a plasma torch with improved energy efficiency and operational stability, enabling more efficient production of high-quality Ti alloy powders for AM applications.

Justification of the prospects for using of reverse polarity plasma torches for plasma atomization of wire materials

It is known that currently, the most common plasma torch designs used for spraying/atomization are single-electrode designs with one cathode and one anode. In such technique the electrode wear leads to significant arc fluctuations, which deteriorates its dynamics [35]. Consequently, the plasma jet pulsations affect process stability, worsening the uniformity of axial and radial velocity and temperature gradients of the plasma jet [36, 37], which results in uneven melting and fragmentation of the wire material with obtaining of a wider particle size distribution dominated by a coarser fraction, as well as a decrease in the sphericity coefficient, etc. Currently, intense electrode wear, led to developing new concepts of high-power plasma torches – multi-electrode type (mainly 3 cathodes and 1 anode) and/or cascaded systems where arc fluctuations do not exceed ±5 V [38–41]. These plasma torches are characterized by increased operational stability and extended service life, as the use of a multi-cathode system reduces current density in each cathode at a constant total arc power, and the use of a cascaded system effectively limits axial displacements of the anode spot, resulting in more stable arc behavior and a virtually constant output power during spraying/atomization [37, 38].

In this aspect, the concept of plasma torches with a copper hollow internal electrode is of interest. These torches can operate on both direct (DPT) and reverse polarity plasma torches (RPT), use both monatomic (argon, helium) and diatomic/multiatomic (nitrogen, hydrogen, methane, etc.) gases and their mixtures as a plasma-forming gas, which allows the formation of supersonic, high-enthalpy plasma jets at low current loads on the internal electrodes [42–44]. Additionally, the application of a non-transferred arc with reverse polarity, where the copper plasma-forming nozzle acts as the cathode and the hollow internal copper electrode acts as the anode [42, 45–47], is a promising direction of plasma torches design. The ability of the cathode spot to actively move in the arc discharge is due to the following physical factors [34, 42, 47–51]:

1. Local overheating of the cathode - the cathode spot concentrates high power on a small area, causing local heating. When the temperature in the spot region exceeds the optimum, the cathode material begins to evaporate, worsening emission conditions. New centers form in colder areas, and old ones disappear.
2. Electromagnetic forces (Ampere force and magnetic compression) - the interaction of the cathode spot current with its own magnetic field creates Lorentz forces, which can lead to spot displacement (especially at currents > 100 A).
3. Gas dynamic influence of the plasma-forming gas can «blow off» the cathode spot, promoting its movement to a region with lower pressure gradient values.

Thus, author's [51] shows that changing the polarity from direct to reverse at constant current leads to arc elongation and allows increasing the arc voltage thereby increasing the output power of the RPT plasma torch. Additionally, in works [30, 51, 52], it is noted that with an increase in plasma torch power, more intense heating of the working gas occurs, leading to an increase in its temperature and a decrease in density. As a result, the gas outflow velocity through the nozzle increases, reaching supersonic values. The authors

showed [52] that the RPT plasma torch operates stably with arc fluctuations which ensures uniform quality of the obtained powders and good reproducibility of the atomization process. Furthermore, compared to a conventional single-cathode argon plasma torch operating on direct polarity, the RPT plasma torch operates at a higher arc voltage and lower current, resulting in less electrode wear. Additionally, the thermal efficiency of the RPT plasma torch and the specific enthalpy of its plasma jet, making it ideal for generating a supersonic plasma jet with high energy density, while low erosion rate of copper electrodes is observed. Thus, the performed analysis confirms the effectiveness and prospects of using RPT plasma torches in PA technology [47, 51, 52]. At the same time, there is a need to improve their design from the point of view of reducing the dispersity of the obtained powders and achieving the required level of their technological properties.

Aim of the work

The aim of this work is to investigate the physical, mechanical and technological properties of titanium alloy Ti-6Al-4V Grade 5 powders obtained by the PA (plasma-arc wire atomization) technique using an DC RPT plasma torch with a copper hollow electrode and a diffusive nozzle-anode. To achieve this goal, it is necessary to:

- confirm the possibility of generating a supersonic plasma jet with the RPT plasma torch and achieving the effect of increasing the dispersity of the obtained powder, compared to plasma-arc wire atomization at subsonic plasma outflow velocities;
- investigate the structure, particle size distribution, morphology, and technological properties of Ti-6Al-4V Grade 5 powder obtained using an RPT plasma torch with the implementation of a supersonic plasma jet mode;
- perform a comparison of the main technological characteristics of Ti-6Al-4V Grade 5 powder obtained using an RPT plasma torch with the implementation of a supersonic plasma jet mode, and justify the prospects of its use in additive manufacturing.

MATERIAL AND METHODS

The experiments were carried out on technological equipment for plasma-arc atomization manufactured by LLC «SPC «PLAZER» (Ukraine) using the PLAZER 180 PL-S unit [53]. For the PA process it was used an experimental RPT plasma torch with a copper hollow electrode (Figure 1b, 1c), operating according to the «non-transferred plasma arc» scheme (NTPA) that has been designed by the E.O. Paton Electric Welding Institute. This plasma torch with an expanding (diffusive) nozzle channel and vortex stabilization of the DC arc allows generating strongly ionized plasma in argon, nitrogen, helium, and their mixtures, including with hydrogen and methane, at atmospheric pressure and currents of 100–400 A, with axial temperature values up to $25–35\times10^3$ K [54, 55]. High-enthalpy plasma jets with plasma-forming gas flow rates in the range of 3–24 m^3/h are created at a large arc length 40–70 mm, which self-adjusts depending on the type of plasma-forming gas and its flow rate, and a high efficiency coefficient $\eta\sim0.7$, which allows effectively heating the plasma-forming gas, increasing its outflow velocity, and forming a supersonic plasma jet. The use of a conical diffusive nozzle reduces arc movement and plasma jet fluctuations to 5–10 V, due to the nozzle geometry providing a hydrodynamically stable plasma flow without formation of large-scale turbulence in the region of the cathode arc attachment on the conical step of the nozzle surface (cathode) [56–58]. This leads to the formation of longer and more stable plasma jets with higher specific enthalpy [56].

In general, the process of plasma-arc atomization of solid wire involves its feeding into a localized high-speed zone of the plasma jet (Figure 1, (a)), where occurs heating, formation of melt on the wire end, its fragmentation, and the formation of primary fragments (droplets).

Subsequent processes of secondary fragmentation of primary droplets, their spheroidization, and solidification occur mainly outside the high-temperature zone of the plasma jet, during its outflow into the surrounding atmosphere. Subsequently, depending on the atomization aim, solidification of secondary droplets (powders) occurs during their free fall inside the reactor of the atomization chamber.

Optimization of the PA process parameters was performed using the results of mathematical modeling and previous experimental research results [59–65]. The technological parameters of the PA process were as follows: current 300 A, operating arc voltage 70–140 V, plasma-forming gas (argon) flow rate 6–15 m^3/h.

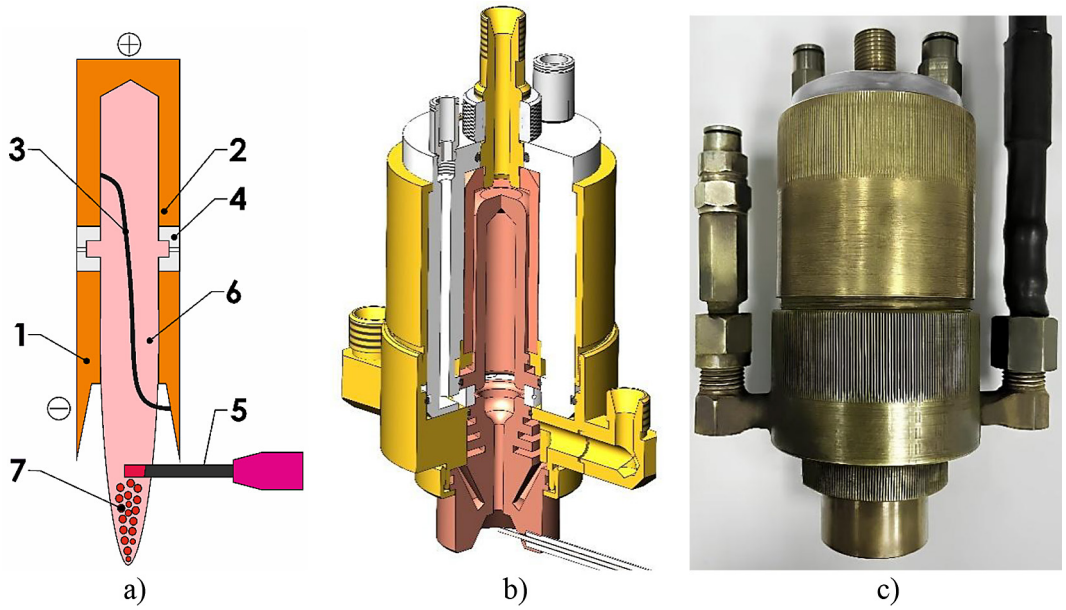

Figure 1. Schematic (a) of PA process of 1.0 mm Ti-6Al-4V Grade 5 solid wire in atomization chamber, 3D model (b) and appearance (c) of RPT plasma torch, where: 1 – expanding plasma-forming nozzle (cathode); 2 – hollow copper electrode (anode); 3 – plasma arc; 4 – swirl ring; 5 – atomized wire; 6 – high-speed plasma jet; 7 – powder

Further solidification of the formed fragments (powders) took place in a laboratory atomization chamber (reactor, Figure 2) in atmosphere of argon, where before filling of atomization chamber by argon, the internal volume of the chamber was evacuated to a residual pressure of 5–7 × 10^{-3} Torr.

A solid wire of Ti-6Al-4V Grade 5 titanium alloy with a diameter of 1.0 mm was used as the feedstock material. The chemical composition of the wire according to the manufacturer certificate is shown in Table 1.

Particle size distribution analysis of the powder was performed by screen sizing according to ISO 2591-1:1988 using an AS-200U (ROTAP) (Ukraine) impact sieve analyzer with a set of sieves with aperture sizes of 25–250 μm. The sample weight was at least 500 g of powder. Morphology of atomized powder was investigated using images from scanning electron microscope (SEM) TESCAN VEGA 3 SBH EasyProbe (Czech Republic) with thermionic electron gun and their subsequent analysis in «MIPAR» software (USA) using the methodology described in [66–70].

Loose powder samples have been mounted on standard holding stubs using carbon adhesive tape. Microstructure of the atomized powder was studied by metallographic analysis. Investigations were carried out using a Carl Zeiss Jena Neophot-32 (Germany) inverted metallographic microscope with a digital camera attachment.

The preparation of metallographic sections was carried out using the following procedure:

1. Cutting samples on a BEUHEL ISOMet 1000 (USA) machine using diamond cut-off blades (Diamond Cut-Off Blade 11-4808E);
2. Embedding samples in resin block, grinding using SiC waterproof abrasive paper with P400, P600 grit, and elastic discs containing diamond inclusions of various particle sizes (A28/14 and A14/10);
3. Polishing on a wool cloth using DiaDuo diamond suspension with a diamond particle size of 3 μm;
4. The reagent composition (%vol.) for revealing the microstructure of the samples was as follows: HF:HNO3:H2O=1:1:1. Before etching, the samples were heated to a temperature of ~50 °C.
5. The phase composition of the powder and the lattice parameters of individual phases were investigated by X-ray diffraction analysis (XRD). X-ray diffraction studies were performed on a DRON-M1 (Ukraine) X-ray diffractometer in monochromatized CuKα radiation. A graphite single crystal installed on the diffracted beam was used as a monochromator. The sample was scanned by the

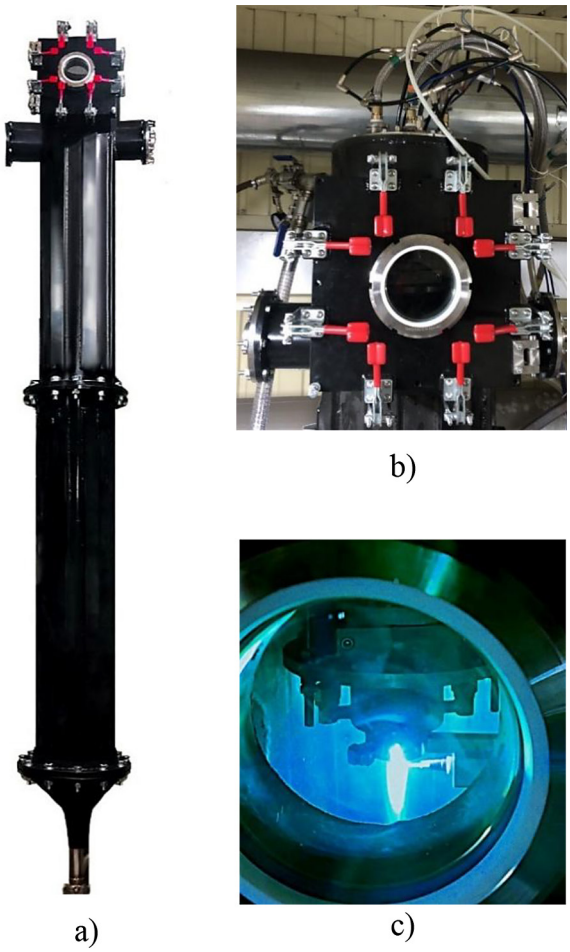

Figure 2. External view of the atomization chamber main components: a - reactor chamber; b - part of the atomization chamber with a service window, plasma torch mounting flange, and vacuum feedthroughs for wire injection; c - visualization of the wire atomization process through the viewport of the atomization chamber.

Bragg-Brentano method in 2Θ geometry. The scanning angle varied from 10° to 120°. The scanning step was 0.05°, and the exposure time was 3–9 s. The processing of diffractometric measurement data was performed using the «PowderCell 2.4» (Germany) program for full-profile analysis of X-ray spectra from a mixture of polycrystalline phase components;

6. Microstructure and chemical composition analysis of the powder was done by using a TESCAN VEGA3 SBH EasyProbe scanning electron microscope. Electron Probe Micro Analysis (EPMA) method was carried out with Bruker Quantax spectrometer (Germany) using XFlash 6–10 energy dispersive spectrometry (EDS) detector;
7. The oxygen and nitrogen content in the atomized powders was investigated using a LECO TC-436 Nitrogen Oxygen Analyzer (USA) gas analyzer;
8. The flowability of the powder was determined using a Hall flowmeter according to the Standard Test Methods for Flow Rate of Metal Powders Using the Hall Flowmeter Funnel ASTM B213-20 standard;
9. Measurement of the powder's bulk density was done according to the Standard Test Method for Apparent Density of Free-Flowing Metal Powders Using the Hall Flowmeter Funnel ASTM B212-21 standard.

RESULTS AND DISCUSSION

Figure 3 shows the appearance of plasma jets generated by the specified plasma torch when using different flow rates of plasma-forming gases (hereinafter referred as G), which contributes to the formation of a subsonic (Figure 3a) at G = 6 m³/h and a supersonic argon jet (Figure 3b) – G = 15 m³/h.

Based on the analysis of the obtained images of the supersonic plasma jet, the Mach number was calculated using the following empirical formula, based on the distance between the shock waves [71]:

$$M \approx \frac{\lambda}{0.67 \cdot d} \approx 2 \qquad (1)$$

where: M is the Mach number; λ is the distance between the shock waves (in this case λ = 8 mm); d is the nozzle diameter (in this case d = 6 mm).

The speed of sound in argon was determined by the following formula without considering ionization excitation of the gas [72]:

Table 1. Chemical composition of the Ti-6Al-4V Grade 5 wire

Chemical composition, wt%							
Ti	Al	V	Fe	C	N	O	H
Bal.	5.87	3.90	0.34	0.020	0.015	0.107	0.003

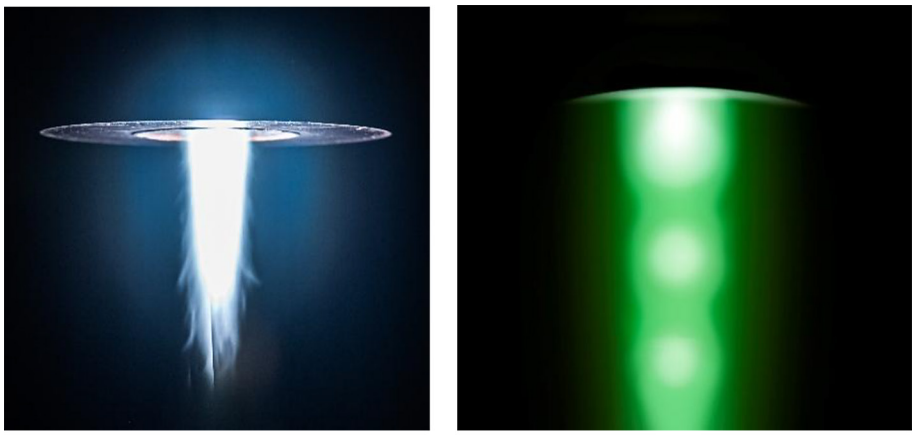

Figure 3. Visualization of plasma jets generated by a RPT plasma torch with a copper hollow electrode during, respectively, subsonic M≈0.8, G = 6 m³/h (a) and supersonic M≈2, G = 15 m³/h (b) outflow of argon plasma into the surrounding atmosphere.

$$a = \sqrt{\gamma RT} = 1440\ m/s \quad (2)$$

where: γ is the adiabatic index (for argon $\gamma \approx 1.67$); R is the gas constant for argon (R = 208.1 J/(kg·K)); T is the temperature of the argon plasma at the nozzle outlet, K (T = 6000 K).

An approximate determination of the gas velocity at the nozzle outlet during its supersonic outflow (flow rate G = 15 m³/h) was performed [72]:

$$V = M \cdot a = 2880\ m/s \quad (3)$$

where: M is the Mach number (M = 2); a – speed of sound in argon (a = 1440 m/s).

According to experimental and calculated data presented in contributions [73, 74], the mean velocity of an argon plasma jet, characteristic of subsonic outflow of the plasma jet at an argon flow rate of G ≈ 6 m³/h and a current of I = 300–400 A, is on average 1200 m/s.

An approximate determination of the Mach number at the nozzle outlet during its, so-called, subsonic outflow was performed [72]:

$$M = \frac{V}{a} \approx 0.8 \quad (4)$$

where: V is the gas velocity at the nozzle outlet at a flow rate of G = 6 m³/h (V = 1200 m/s); a is the speed of sound in argon (a = 1440 m/s).

Thus, increasing the flow rate of the plasma-forming gas from 6 to 15 m³/h leads to an increase in the plasma jet outflow velocity at the plasma-forming nozzle outlet from M = 0.8 to M = 2.0.

Figure 4 shows the results of the particle size distribution for powders obtained during subsonic and supersonic outflow of the argon jet, where the change in the plasma flow regime achieved by increasing the argon flow rate from G = 6 m³/h to 15 m³/h, with nozzle configuration and current unchanged. The obtained results observed, that the formation of a supersonic plasma jet significantly increases the yield of the fine powder fraction. At a flow rate of G = 15 m³/h, the yield of the fine fraction -63 μm reaches up to 55 wt%, whereas in the case of subsonic plasma jet flow (G = 6 m³/h) the yield does not exceed 30 wt%. Furthermore, under supersonic atomization mode, the average powder diameter is d_{50} = 63 μm, compared to d_{50} = 104 μm in the subsonic mode.

The reduction of the average powder diameter d_{50} by 39% using supersonic flow and the formation of significantly smaller powders that due to increasing gas-dynamic pressure on the melt, which formed during the melting of the ends of the atomized wires [30, 32, 33]. Increasing the volumetric flow rate of the plasma-forming gas will be increase the outflow velocity of the plasma jet, which leads to effective fragmentation of the melt at the wire end. Thus, the ratio of plasma-forming gas/molten metal is an important parameter that allows controlling the powder size during the plasma wire atomization process.

According to economic numbers the most productive regime to atomize materials, among the methods studied, is by using a plasma-forming

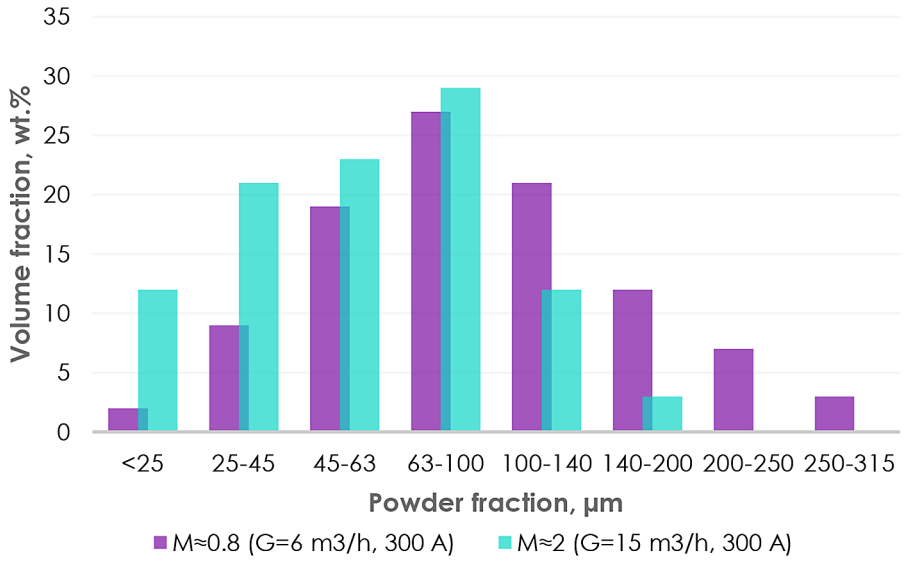

Figure 4. Particle size distribution of PA powder from Ti-6Al-4V Grade 5 titanium alloy, obtained at subsonic plasma jet outflow velocity (a) – Mach number M≈0.8, and under supersonic conditions (b) – Mach number M≈2

gas flow rate of 6 m³/h, which yields a productivity of 2.4 kg/h at a plasma torch power of 27 kW. Also, increasing the argon flow rate to G = 15 m³/h at a constant current of 300 A leads to an increase in arc voltage from 90 to 140 V and, accordingly, to an increase in plasma torch power to 42 kW. However, these results will be decreasing the process productivity to 1.8 kg/h, which may be due to plasma cooling, a decrease in its enthalpy and temperature [34].

Figure 5 shows SEM images of PA powders from Ti-6Al-4V Grade 5 titanium alloy with fractions +45;-106 µm (Figure 5a) and +63;-160 µm (Figure 5c) and the results of processing the obtained images in the «MIPAR» software product (Figure 5b, 5d).

Analysis of the morphology of titanium powder in MIPAR showed that the +45;-106 µm fraction powder has a spherical shape with an average sphericity coefficient S = 0.91, and for the +63;-160 µm fraction, S = 0.87, while the proportion of powder with defects in the form of satellites and irregularly shaped particles does not exceed 2 wt%.

Figure 6 shows images of the cross-section of the -100 µm fraction powder particles (Figure 6a) and the +100;-160 µm fraction powder particles (Figure 6(b-d)). Analysis of the obtained images showed that the microstructure for all powder fractions is characterized by the absence of pores and voids inside the powder, which is inherent for gas atomization. Such a difference between the structural properties of powders obtained by PA and GA techniques is due to the following [15, 17, 18, 20]:

- PA is characterized by less gas entrapment due to lower gas dynamic influence on the metal melt, as the gas pressure in the atomization process does not exceed 4–10 bar, while for GA methods, the pressure values are at least 20–40 bar with its turbulent outflow character;
- PA is characterized by high gas temperatures at the nozzle outlet of plasma torch (in general, the gas temperature lies in the range of 4,000–10,000 °C), which contributes to a long residence time of the powder in the «hot» state, which, when presence of gas inside the powder, promotes its complete release, unlike the GA process, where cold gas is used to atomize the melt, which promotes instantaneous solidification of the powder and the inability to degas its internal volume.

Figure 7 shown the characteristic spectra of atomized powders of various fractions by EPMA with energy dispersive spectrometry. Numerous results of analysis are represented together with analysis of the initial feedstock (wire) in the Table 2. It is shown that obtained powders meets the requirements for the chemical composition of wires and rods from titanium alloys according to the ASTM B348-05 standard «Standard

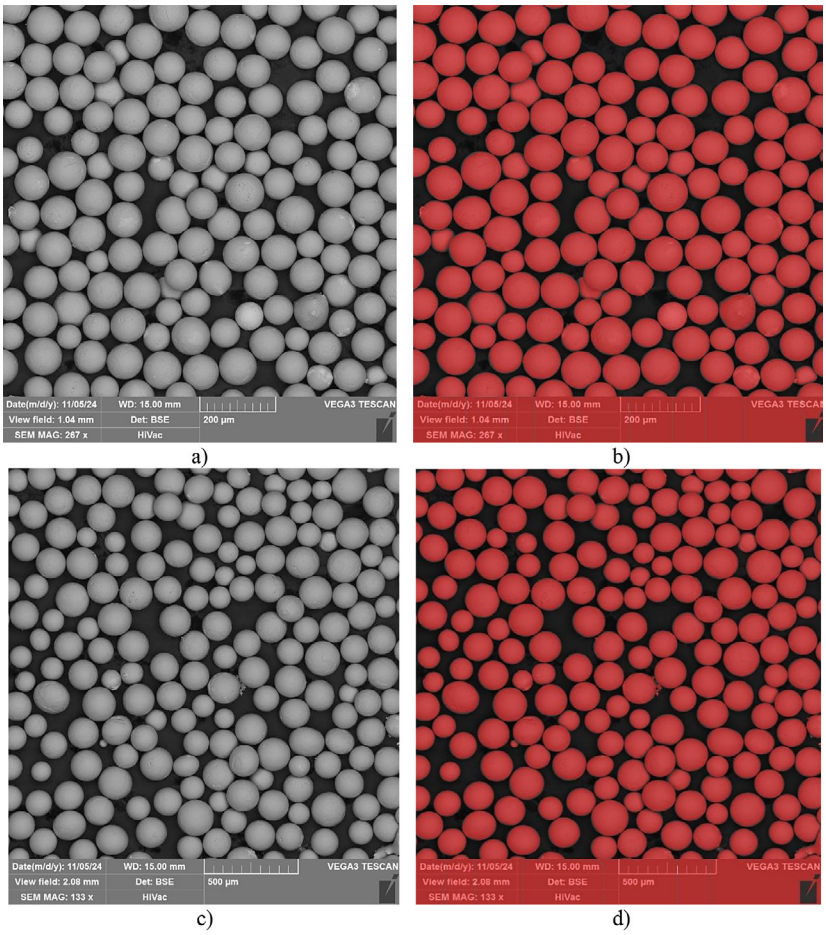

Figure 5. SEM images of Ti-6Al-4V Grade 5 titanium alloy powder with fractions +45;-106 µm (a) and +63;-160 µm before (a, c) and after processing in the MIPAR software product (b, d)

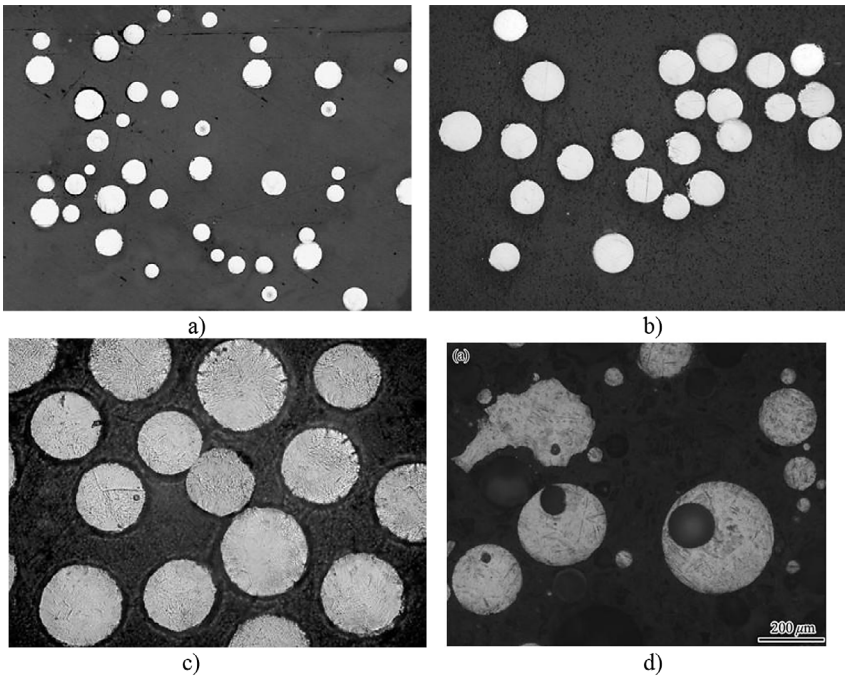

Figure 6. Microstructure of Ti-6Al-4V Grade 5 powder of the classes -100 µm (a) and +100;-160 µm (b, c, where c – chemical etching using etchant solution HF:HNO_3:H_2O=1:1:1) obtained by developed technique as well as powder of the class +100;-160 µm [75], obtained by GA-EIGA technique (d)

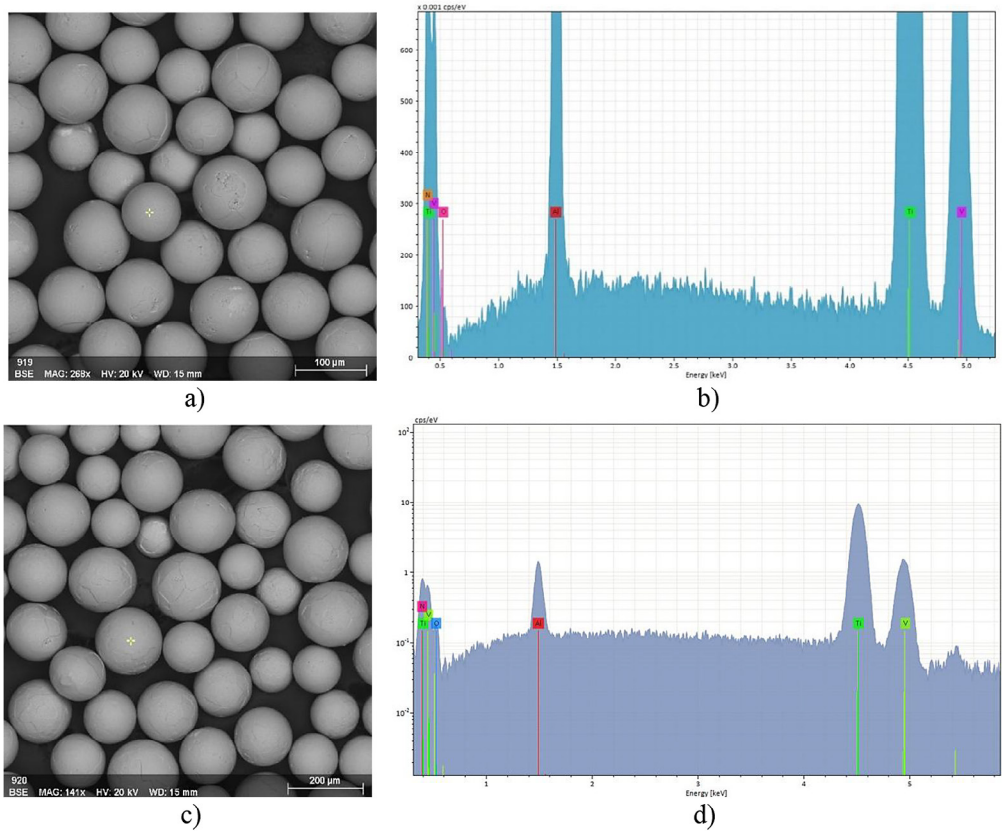

Figure 7. Location of the analyzed areas (a, c) on the SEM image and the results of EPMA analysis (b, d) of the -100 µm fraction powder (a, b) and +100;-160 µm (c, d)

Table 2. Results of local chemical composition analysis of the initial wire and atomized powders of various fractions by EDS

No.	Specimen	Chemical composition, %			
		Ti	Al	V	Fe
1	Element content according to ASTM B348 05	bal.	5.5–6.75	3.5–4.5	0.4
2	Initial wire	bal.	5.87	3.90	0.34
3	Powder fraction -100 µm	bal.	5.67	3.72	0.35
4	Powder fraction +100; -160 µm	bal.	5.84	3.69	0.31

specification for titanium and titanium alloy bars and billets».

The study of oxygen and nitrogen content in atomized powders (Table 3) showed that the chemical composition in terms of oxygen and nitrogen meets the requirements for the chemical composition of wires and rods made of titanium alloys according to the ASTM B348-05 standard «Standard specification for titanium and titanium alloy bars and billets».

Results of the X-ray diffraction analysis (Figure 8, Table 4) showed that the phase composition of the powder for all fractions consists mainly of α-Ti, however, for the coarse fraction of the +160;-250 µm powder, a small amount of 3.55 vol.% β-Ti is detected.

Table 5 shows the technological properties of commercial and investigated Ti-6Al-4V Grade 5 titanium alloy powders of various fractions, obtained by GA-VIGA, supreme-speed plasma rotating electrode process (SS-PREP) and PA-3DPT atomization techniques. The high sphericity of the investigated powders determines their high technological properties, which are closely equivalent to properties of powders obtained by SS-PREP and PA-3DPT technologies. At the same time, the technological properties of the obtained powder exceed the

Table 3. Study of oxygen and nitrogen content in the initial wire and atomized powder of various fractions

No.	Specimen	Oxygen (wt%)	Nitrogen (wt%)
1	Element content according to ASTM B348 05	0.20 max	0.05 max
2	Initial wire	0.19	0.0078
3	Powder fraction -100 μm	0.17	0.0050
4	Powder fraction +100; -160 μm	0.17	0.0057
5	Powder fraction +160; -250 μm	0.19	0.0050

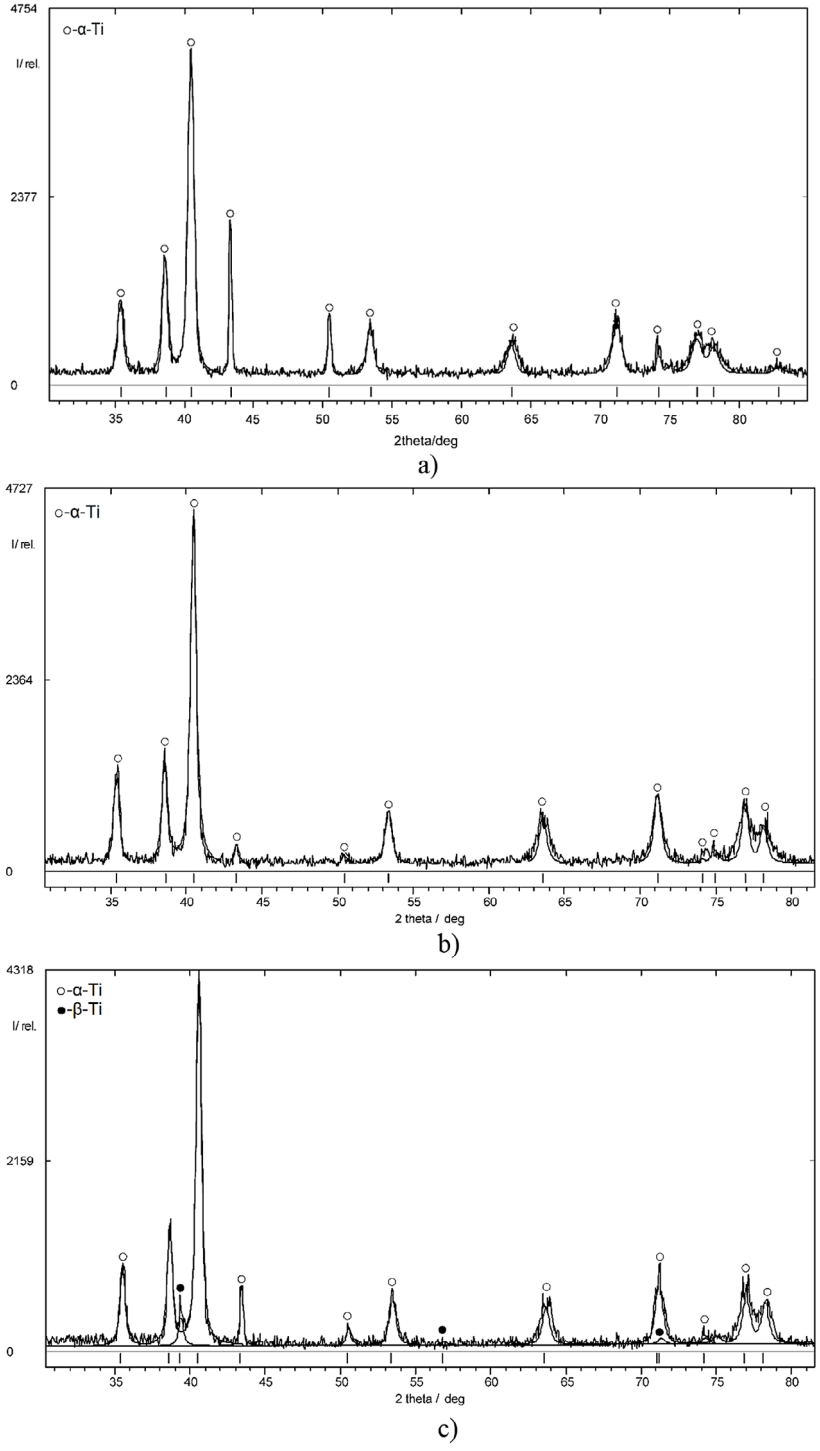

Figure 8. Diffraction patterns of Ti-6Al-4V Grade 5 titanium alloy powders of fractions -100 μm (a), +100;-160 μm (b) and -160;+250 μm (c)

Table 4. Results of XRD analysis of Ti-6Al-4V Grade 5 titanium alloy powders of fractions –100 μm, +100;-160 μm and –160;+250 μm

No.	Specimen	Phases	Phase cont., %vol.	Lattice parameters, Å
1	Powder fraction -100 μm	α-Ti	100	a=2.9213; c=4.6524; c/a=1.592
		β-Ti	-	-
2	Powder fraction +100; -160 μm	α-Ti	100	a=2.9242; c=4.6599; c/a=1.593
		β-Ti	-	-
3	Powder fraction +160; -250 μm	α-Ti	96.46	a=2.9253; c=4.6524; c/a=1.590
		β-Ti	3.55	a=4.6659

Table 5. Technological properties of Ti-6Al-4V Grade 5 titanium powder obtained by various atomization technologies

Manufacturing technique	Class, μm	Bulk density, g/cm^3	Flowability, s/50 g
GA-VIGA (Höganäs, Sweden) [76]	+45;-100	2.35	<35
	+63;-160	2.38	<29
SS-PREP (Sino-Euro, China) [77]	+45;-100	2.40–2.60	<30
	+63;-160	2.50–2.70	<25
PA-3DPT (AP&C, USA) [78]	+45;-100	2.52	<28
	+63;-160	2.59	<25
PA-RPT (PEWI, Ukraine)	+45;-100	2.46	<31
	+63;-160	2.51	<26

technological properties of GA-VIGA powder in terms of flowability and bulk density.

Improvement of the technological properties of PA-RPT powder, compared to GA, is explained by the absence of external defects in the form of satellites and better sphericity. These external defects and shape imperfections leads to increased adhesion and internal friction between powder particles, which is associated with increased unevenness and an increased contact area between particles, which somewhat worsens the flowability and bulk density characteristics [20].

CONCLUSIONS

1. By PA-RPT atomization of Ti-6Al-4V Grade 5 as an example, it has been experimentally confirmed that generating a supersonic plasma jet with a Mach number of approximately M≈2 using an RPT plasma torch with a copper hollow electrode, compared to its subsonic outflow (Mach number M≈0.8), contributes to a 40% reduction in the average diameter d_{50} of the obtained powder, specifically from 104 to 63 μm. In this case content of the fine fraction -63 μm increases from 30 to 55 wt%.
2. Ti-6Al-4V Grade 5 powder, obtained by wire atomization by supersonic plasma jets using an RPT plasma torch in a chamber with controlled atmosphere (argon with preliminary vacuuming to 5–7×10^{-3} Torr), is characterized by a high sphericity coefficient (at the level of 0.9), and practically lacks defects in the form of satellites, irregular-shaped particles, and internal porosity. Chemical composition analysis of the powder showed its complete correspondence to the chemical composition of the initial material – the wire. The main phase of the powder is α-Ti, but for the coarse fraction +160; -250 μm, 3.55 wt% of β-Ti is identified.
3. It was confirmed that in terms of technological characteristics (particle size distribution, bulk density, flowability), Ti-6Al-4V Grade 5 powder obtained by supersonic plasma wire atomization with an RPT plasma torch is on par with the industrial techniques of obtaining spherical powders for AM – SS-PREP (with rotation speeds exceeding 30,000 rpm) and PA-3DPT techniques, and surpasses the technological properties of powders of similar composition produced via GA-VIGA. This implies a great prospect for using powders obtained with the developed RPT plasma torch in AM, primarily in SLM, CS, EBM, and LDED processes.

Acknowledgments

The research was funded within the following programs:

1. The GDAS'Project of Science and Technology Development [2020GDASYL-20200301001];
2. The National Key Research and Development Program of China [2020YFE0205300].

REFERENCES

1. Nguyen, H., Pramanik, A., Basak, A. et al. A critical review on additive manufacturing of Ti-6Al-4V alloy: microstructure and mechanical properties. Journal of Materials Research and Technology. 2022; (18), 4641–4661. https://doi.org/10.1016/j.jmrt.2022.04.055
2. Del Guercio, G., Galati, M., Saboori, A. Electron beam melting of Ti-6Al-4V lattice structures: correlation between post heat treatment and mechanical properties. Int J Adv Manuf Technol. 2021; (116), 3535–3547. https://doi.org/10.1007/s00170-021-07619-w
3. Kondas, J., Guagliano, M., Bagherifard, S. et al. Cold spray additive manufacturing of Ti6Al4V: Deposition optimization. J Therm Spray Tech 2024; (33), 2672–2685. https://doi.org/10.1007/s11666-024-01855-8
4. Weng, F., Bi, G., Chew, Y. et al. Robust interface and excellent as-built mechanical properties of Ti–6Al–4V fabricated through laser-aided additive manufacturing with powder and wire. Int J Miner Metall Mater. 2025; (32), 154–168. https://doi.org/10.1007/s12613-024-3003-8
5. Len, E., Galstian, I., Gustmann, T. et al. Effect of high energy laser processing on defect and structural phase state of titanium products made by additive technologies. Appl. Phys. A 2025; 131, 187. https://doi.org/10.1007/s00339-025-08303-6
6. Gu, Y., Xu, Y., Shi, Y. et al. Corrosion resistance of 316 stainless steel in a simulated pressurized water reactor improved by laser cladding with chromium. Surface and Coatings Technology. 2022; (441), 128534. https://doi.org/10.1016/j.surfcoat.2022.128534
7. Mao, D., Xie, Y., Meng, X. et al. Strength-ductility materials by engineering a coherent interface at incoherent precipitates. Materials Horizons. 2024; (14), 3408–341920. https://doi.org/10.1039/d4mh00139g
8. Ahn, D. Directed Energy Deposition (DED) Process: State of the Art. Int. J. of Precis. Eng. and Manuf.-Green Tech. 2021; (8), 703–742. https://doi.org/10.1007/s40684-020-00302-7
9. Svetlizky, D., Das, M., Zheng, B. et al. Directed energy deposition (DED) additive manufacturing: Physical characteristics, defects, challenges and applications. Materials Today. 2021; (49), 271–295. https://doi.org/10.1016/j.mattod.2021.03.020
10. King, W., Anderson, A., Ferencz, R. et al. Laser powder bed fusion additive manufacturing of metals; physics, computational, and materials challenges. Applied Physics Reviews. 2015; (2), 041304 https://doi.org/10.1063/1.4937809
11. Kvasnytskyi, V., Korzhyk, V., Kvasnytskyi, V. et al. Designing brazing filler metal for heat-resistant alloys based on Ni_3Al intermetallide. Eastern-European Journal of Enterprise Technologies. 2020; (108), 6–19. https://doi.org/10.15587/1729-4061.2020.217819
12. Hryhorenko, G., Adeeva, L., Tunik, A. et al. Structurization of coatings in the plasma arc spraying process using B_4C + $(Cr, Fe)_7C_3$-cored wires. Powder Metall. Met. Ceram. 2019; (58), 312–322. https://doi.org/10.1007/s11106-019-00080-1
13. Chen, G., Zhao S., Tan P. et al. A comparative study of Ti-6Al-4V powders for additive manufacturing by gas atomization, plasma rotating electrode process and plasma atomization. Powder Technology. 2018; (333), 38–46. https://doi.org/10.1016/j.powtec.2018.04.013
14. Sun, P., Fang, Z., Zhang, Y. et al. Review of the methods for the production of spherical Ti and Ti alloy powder. JOM. 2017; (69), 1853–1860. https://doi.org/10.1007/s11837-017-2513-5
15. Wang, P., Li, X., Zhou, X. et al. Numerical simulation on metallic droplet deformation and breakup concerning particle morphology and hollow particle formation during gas atomization. Transactions of Nonferrous Metals Society of China. 2024; (34), 2074–2094. https://doi.org/10.1016/S1003-6326(24)66526-X
16. Yodoshi, N., Endo, T., Masahashi, N. Evaluation of porosity in gas-atomized powder by synchrotron X-ray CT and investigation of the effect of gas species, Materials Transactions. 2021; (62), 1549–1555. https://doi.org/10.2320/matertrans.MT-Y2021001
17. Wu, J., Xia, M., Wang, J. et al. Effect of electrode induction melting gas atomization on powder quality: satellite formation mechanism and pressure. Materials. 2023; 16, 2499. https://doi.org/10.3390/ma16062499
18. Zhang, L., Xu, W., Li, Z. et. al. Mechanism of rapidly solidified satellites formation in gas atomized powders: Simulation and characterization. Powder Technology. 2023; (418), 118162. https://doi.org/10.1016/j.powtec.2022.118162
19. Luo, S., Wei, Q., Ouyang, Y. et al. The impact of coaxial gas technology on the morphology of powder by gas atomisation and the additive manufactured mechanical performance. Virtual and Physical

Prototyping. 2024; 1, e2375107. https://doi.org/10.1080/17452759.2024.2375107

20. Brika, S., Letenneur, M., Dion, C. et al. Influence of particle morphology and size distribution on the powder flowability and laser powder bed fusion manufacturability of Ti-6Al-4V alloy. Additive Manufacturing. 2019; 100929. https://doi.org/10.1016/j.addma.2019.100929
21. Mathias, L., Pinotti, V., Batistão, B. et al. Metal powder as feedstock for laser-based additive manufacturing: From production to powder modification. Journal of Materials Research. 2024; (39), 19–47. https://doi.org/10.1557/s43578-023-01271-8
22. Kan, W., Chiu, L., Lim, C. et al. A critical review on the effects of process-induced porosity on the mechanical properties of alloys fabricated by laser powder bed fusion. Journal of Materials Science. 2022; (57), 9818–9865. https://doi.org/10.1007/s10853-022-06990-7
23. Al-Maharma, Y., Patil, S., Markert, B. Effects of porosity on the mechanical properties of additively manufactured components: a critical review. Mater. Res. Express. 2020; (7), 122001. https://doi.org/10.1088/2053-1591/abcc5d
24. Liu, Y., Zhao, X., Lai, Y. et al. A brief introduction to the selective laser melting of Ti-6Al-4V powders by supreme-speed plasma rotating electrode process. Progress in Natural Science: Materials International. 2020; (30), 94–99. https://doi.org/10.1016/j.pnsc.2019.12.004
25. Li, H., Zhang, S., Chen, Q. et al. High-quality spherical silver alloy powder for laser powder bed fusion using plasma rotating electrode process. Micromachines. 2024; (15), 396. https://doi.org/10.3390/mi15030396
26. Korzhyk, V., Kulak, L., Shevchenko, V. et al. New equipment for production of super hard spherical tungsten carbide and other high-melting compounds using the method of plasma atomization of rotating billet. Materials Science Forum. 2017; (898), 1485–1497. https://doi.org/10.4028/www.scientific.net/msf.898.1485
27. Cui, Y., Zhao, Y., Numata, H. et al. Effects of process parameters and cooling gas on powder formation during the plasma rotating electrode process. Powder Technology. 2021; (393), 301–311. https://doi.org/10.1016/j.powtec.2021.07.0624
28. Fan, X., Tian, Q., Chu, X. et al. Microstructure and mechanical properties of Co31.5Cr7Fe30Ni31.5 high-entropy alloy powder produced by plasma rotating electrode process and its applications in additive manufacturing. Journal of Materials Research and Technology. 2024; (31), 1924–1938. https://doi.org/10.1016/j.jmrt.2024.06.217
29. Yurtukan, E., Unal, R. Theoretical and experimental investigation of Ti alloy powder production using low-power plasma torches. Transactions of Nonferrous Metals Society of China. 2022; (32), 175–191. https://doi.org/10.1016/S1003-6326(21)65786-2
30. Prokopov, V., Fialko, N., Sherenkovskaya, G. et al. Effect of the coating porosity on the processes of heat transfer under, gas-thermal atomization. Powder Metall. Met. Ceram. 1993; (32), 118–121. https://doi.org/10.1007/BF00560034
31. Zhang, Q., Yu, D., Liu, F. et al. Modeling on the size of the pre-breaking molten droplet in plasma atomization for controlling the size of the produced powders. Applied Thermal Engineering. 2023; (232), 121031. https://doi.org/10.1016/j.applthermaleng.2023.121031
32. Qiu, J., Yu, D., Qu, Y. et al. In-flight droplet plasma atomization: A novel method for preparing ultrafine spherical powders. Advanced Powder Technology. 2025; (36), 104757. https://doi.org/10.1016/j.apt.2024.104757
33. Boulos, M., Fauchais, P., Pfender, E. Handbook of thermal plasmas. Springer International Publishing. 2016. https://doi.org/10.1007/978-3-319-12183-3
34. Mauer, G. Multiple electrodes and cascaded nozzles: A review of the evolution of modern plasma spray torches. J Therm Spray Tech. 2024; (34), 484–494. https://doi.org/10.1007/s11666-024-01909-x
35. Coudert, J., Planche, M., Fauchais, P. Characterization of DC plasma torch voltage fluctuations. Plasma Chem Plasma Process. 1995; (16), 211–227. https://doi.org/10.1007/BF01512636
36. Duan, Z., Heberlein, J. Arc instabilities in a plasma spray torch. J Therm Spray Tech. 2002; (11), 44–51. https://doi.org/10.1361/105996302770348961
37. Schein, J., Zierhut, J., Dzulko, M. et al. improved plasma spray torch stability through multi-electrode design, contrib. Plasma Phys. 2007; (7), 498–504. https://doi.org/10.1002/ctpp.200710064
38. Marque´s, J., Forster, G., Schein, J. Multi-electrode plasma torches: motivation for development and current state-of-the art. Open Plasma Phys. J. 2009; (2), 89–98. https://10.2174/1876534300902010089
39. Perambadur, J., Rat, V., Niane, T. Simulation of the axial III plus plasma torch and its arc fluctuations. J Therm Spray Tech. 2024; (33), 2526–2547. https://doi.org/10.1007/s11666-024-01827-y
40. Zimmermann, S., Mauer, G., Rauwald, K. et al. Characterization of an axial-injection plasma spray torch. J Therm Spray Tech. 2021; (30), 1724–1736. https://doi.org/10.1007/s11666-021-01235-6
41. Dombrovskii, L., Isakaev, E., Senchenko, V. et al. Efficiency of particle acceleration, heating, and melting in high-enthalpy plasma jets. High Temp. 2012; (50), 145–153. https://doi.org/10.1134/S0018151X12020046
42. Yang, I., Choi, M., Nam, J. et al. Experimental and

numerical analyses of a hollow electrode plasma torch with inter-electrodes and reversed polarity discharges. J Korean Phys Soc. 2019; (5), 465–472. https://doi.org/10.3938/jkps.74.465

43. Park, S., Kim, D., Kim, M. et al. Numerical analysis of a hollow electrode plasma torch with a reversed polarity discharge for radioactive waste treatment. Journal of the Korean Physical Society. 2013; (63), 1746–1754. https://doi.org/10.3938/jkps.63.1746
44. Camacho, S. Industrial-worthy plasma torches: State-of-the-art. Pure Appl. Chem. 1988; (60), 619–632. https://doi.org/10.1351/pac198860050619
45. Yin, Z., Yu, D., Wen, Y. et al. Numerical investigation on the flow characteristics of a reverse-polarity plasma torch by two-temperature thermal non-equilibrium modelling. Plasma Science and Technology. 2021; (9), 95402–095402. https://doi.org/10.1088/2058-6272/ac0770
46. Rao, L., Rivard, F., Carabin, P. Thermal plasma torches for metallurgical applications. 4th international symposium on high-temperature metallurgical processing. 2013; 57–65. https://doi.org/10.1002/9781118663448.ch8
47. Lyubimov, G., Rakhovskii, V. The cathode spot of a vacuum arc. Soviet Physics Uspekhi. 1978; (21), 693–718. https://doi.org/10.1070/PU1978v021n08ABEH005674
48. Brilhac, J., Pateyron, B, Coudert J. et al. Study of the dynamic and static behavior of de vortex plasma torches: Part II: well-tye cathode. Plasma Chem Plasma Process. 1995; (15), 257–277. https://doi.org/10.1007/BF01459699
49. Beilis, I. Plasma and Spot Phenomena in Electrical Arcs. Springer Nature. (2020).
50. Min, H., Cho, H., Hong, S. Numerical analysis and experiment on a plasma torch with hollow electrodes for hazardous waste treatment. Ann NY Acad Sci. 1999; (891), 49–56. https://doi.org/10.1111/j.1749-6632.1999.tb08751.x
51. Yin, Z., Yu, D., Zhang, Q. et al. Experimental and numerical analysis of a reverse-polarity plasma torch for plasma atomization. Plasma Chem Plasma Process. 2021; (41), 1471–1495. https://doi.org/10.1007/s11090-021-10181-8
52. The equipment for supersonic plasma spraying of PLAZER 50-PL, PLAZER 80-PL-S and PLAZER 180-PL-S. http://www.plazer.com.ua/en/plazer-50-pl-plazer-80-pl-s-and-plazer-180-pl-s.html
53. Gadzhiev, M., Kulikov, Y., Son, E. et al. Efficient generator of low-temperature argon plasma with an expanding channel of the output. High Temp. 2020; (58), 12–20. https://doi.org/10.1134/S0018151X2001006X
54. Li, K., Zhu, C., Zhang, Y. et al. Experimental study of the discharge characteristics of a stepped-nozzle arc plasma torch. Plasma Chem Plasma Process. 2024; (44), 1469–1492. https://doi.org/10.1007/s11090-024-10481-9
55. Gadzhiev, M., Kulikov, Y., Panov, V. et al. Supersonic plasmatron nozzle profiling with the real properties of high temperature working gas. High Temp. 2016; (54), 38–45. https://doi.org/10.1134/S0018151X15060073
56. Su, G., Shi, Y. Li, G. et al. Improving the deposition efficiency and mechanical properties of additive manufactured Inconel 625 through hot wire laser metal deposition. Journal of Materials Processing Technology. 2023; (322), 118175. https://doi.org/10.1016/j.jmatprotec.2023.118175
57. Gu, Y., Xu, Y., Shi, Y. et al. Corrosion resistance of 316 stainless steel in a simulated pressurized water reactor improved by laser cladding with chromium. Surface and Coatings Technology. 2022; (441), 128534. https://doi.org/10.1016/j.surfcoat.2022.128534
58. Kvasnytskyi, V., Korzhyk, V., Kvasnytskyi, V. et al. Designing brazing filler metal for heat-resistant alloys based on Ni_3Al intermetallide. Eastern-European Journal of Enterprise Technologies. 2020; (108), 6–19. https://doi.org/10.15587/1729-4061.2020.217819
59. Skorokhod, A., Sviridova, I., Korzhik, V. The effect of mechanical pretreatment of polyethylene terephthalate powder on the structural and mechanical properties of coatings made from it. Mekhanika Kompozitnykh Materialov. 1994; 30(4), 455–463.
60. Prokopov, V., Fialko, N., Sherenkovskaya, G. et al. Effect of the coating porosity on the processes of heat transfer under, gas-thermal atomization. Powder Metall. Met. Ceram. 1993; (32), 118–121. https://doi.org/10.1007/BF00560034
61. Fialko, N., Prokopov, V., Meranova, N. et al. Temperature conditions of particle-substrate systems in a gas-thermal deposition process. Fizika i Khimiya Obrabotki Materialov. 1994; (2), 59–67.
62. Fialko, N., Prokopov, V., Meranova, N. et al. Thermal physics of gas thermal coatings formation processes. State of investigations. Fizika i Khimiya Obrabotki Materialov. 1993; (4), 83–93.
63. Jing, H., Yu, Shi, Gang, Z. et al. Minimizing defects and controlling the morphology of laser welded aluminum alloys using power modulation-based laser beam oscillation. J. Manufacturing Processes. 2022; (83), 49–59. https://doi.org/10.1016/j.jmapro.2022.08.031
64. Skorokhod, A., Sviridova, I., Korzhik, V. Structural and mechanical properties of polyethylene terephthalate coatings as affected by mechanical pretreatment of powder in the course of preparation. Mekhanika Kompozitnykh Materialov. 1994; (30), 455–463.

65. Fialko, N., Dinzhos, R., Sherenkovskii, J. et al. establishing patterns in the effect of temperature regime when manufacturing nanocomposites on their heat-conducting properties. Eastern-European Journal of Enterprise Technologies. 2021; (112), 21–26. https://doi.org/10.15587/1729-4061.2021.236915
66. Korzhik, V. Theoretical analysis of amorphization conditions for metallic alloys under gas-thermal spraying. III. Transformations in the amorphized alloy underbuilding-up of coatings. Powder Metall Met Ceram. 1992; (31), 943–948. https://doi.org/10.1007/BF00797621
67. Fialko, N., Dinzhos, R., Sherenkovskii, J. et al. Establishment of regularities of influence on the specific heat capacity and thermal diffusivity of polymer nanocomposites of a complex of defining parameters. Eastern-European Journal of Enterprise Technologies. 2021; (114), 34–39. https://doi.org/10.15587/1729-4061.2021.245274
68. Fialko, N., Dinzhos, R., Sherenkovskii, J. et al. Influence on the thermophysical properties of nanocomposites of the duration of mixing of components in the polymer melt. Eastern-European Journal of Enterprise Technologies. 2022; (116), 25–30. https://doi.org/10.15587/1729-4061.2022.255830
69. Gu, Y., Zhang, W., Xu, Y. et al. Stress-assisted corrosion behaviour of Hastelloy N in FLiNaK molten salt environment. npj Mater Degrad. 2022; (6), 90. https://doi.org/10.1038/s41529-022-00300-x
70. Zhukov, M., Zasypkin, I. Thermal Plasma Torches. Cambridge International Science Publishing Ltd. 2007.
71. Landau, L., Lifshitz, E. Physical kinetics. Pergamon Press Ltd. 1981.
72. Bobzin, K., Heinemann, H., Dokhanchi, A. Numerical and Experimental Analysis of a Solid Shroud in Multi-arc Plasma Spraying. J Therm Spray Tech. 2024; (33), 1191–1204. https://doi.org/10.1007/s11666-024-01715-5
73. Wen, K., Liu, X., Liu, M. et. al. Numerical simulation and experimental study of Ar-H_2 DC atmospheric plasma spraying. Surface and Coatings Technology. 2019; (371), 312–321. https://doi.org/10.1016/j.surfcoat.2019.04.053
74. Guo, R., Xu, L., Zong, B. et al. Characterization of Prealloyed Ti–6Al–4V Powders from EIGA and PREP Process and Mechanical Properties of HIPed Powder Compacts. Acta Metall. Sin. (30), 2017; 735–744. https://doi.org/10.1007/s40195-017-0540-4
75. https://www.hoganas.com/en/powder-technologies/additive-manufacturing-metal-powders/3d-printing-metal-powders/titanium-alloy-am-powders/
76. https://en.c-semt.com/ti/
77. https://www.advancedpowders.com/powders/titanium-alloys/ti-6al-4v-grade-5